Journal of
Marine Science and Engineering

MDPI

Article

Scour Protection of Submarine Pipelines Using Ionic Soil Stabilizer Solidified Soil

Ruigeng Hu [1], Xiuhai Wang [1,2,3,*], Hongjun Liu [1,2,3] and Hao Leng [1]

[1] College of Environmental Science and Engineering, Ocean University of China, Qingdao 266000, China; huruigeng@stu.ouc.edu.cn (R.H.); hongjun@ouc.edu.cn (H.L.); lh4517@stu.ouc.edu.cn (H.L.)
[2] Key Lab of Marine Environment and Ecology, Ministry of Education, Ocean University of China, Qingdao 266000, China
[3] Key Laboratory of Shandong Province for Marine Environment and Geological Engineering, Ocean University of China, Qingdao 266000, China
* Correspondence: showseas@ouc.edu.cn

Abstract: A novel scour protection approach for pipeline using the Ionic Soil Stabilizer (ISS) solidified soil was proposed in this study. The ISS-solidified slurry can be poured adjacent to the pipeline immediately after it was placed, or in the growing scour holes. In the present study, the first type was utilized as the scour protection layer around the pipeline. A series of laboratory flume tests were conducted to validate the protective capacity of ISS-solidified slurry for the pipeline in waves and combined waves and current. Then, the scanning electron microscope (SEM) tests and pore size tests were carried out, respectively, to investigate the mechanism of ISS-solidified slurry for scour protection around the pipeline. Finally, the effects of the ISS-solidified layer for liquefaction stability of non-cohesive subsoil were evaluated. The results indicated that the ISS-solidified slurry is a reliable, economic approach for scour protection around pipelines in the ocean environment. It is noteworthy that if a non-cohesive soil layer underlies the ISS-solidified slurry, it is vulnerable to suffer accumulated liquefaction due to the dense crust structure of the ISS-solidified layer, so the adverse effects for accumulated liquefaction should be considered carefully due to the set of the ISS-solidified layer.

Keywords: scour protection; pipeline; ionic soil stabilizer (ISS); scour tests

check for updates

Citation: Hu, R.; Wang, X.; Liu, H.; Leng, H. Scour Protection of Submarine Pipelines Using Ionic Soil Stabilizer Solidified Soil. *J. Mar. Sci. Eng.* **2022**, *10*, 76. https://doi.org/10.3390/jmse10010076

Academic Editor: Eva Loukogeorgaki

Received: 9 December 2021
Accepted: 4 January 2022
Published: 7 January 2022

Publisher's Note: MDPI stays neutral with regard to jurisdictional claims in published maps and institutional affiliations.

Copyright: © 2022 by the authors. Licensee MDPI, Basel, Switzerland. This article is an open access article distributed under the terms and conditions of the Creative Commons Attribution (CC BY) license (https://creativecommons.org/licenses/by/4.0/).

1. Introduction

Submarine pipelines are widely adopted to transport the oil, gas, hydrocarbons and other liquids in ocean engineering [1,2]. When a pipeline is placed on the seabed, it will suffer the action of waves and current, resulting in the local scour occurring in the vicinity of the pipeline [3,4]. As the scour pit evolves along the pipeline, it will span the scour pit. If the free span is long enough, the pipeline begins to sag, leading to pipeline instability and failure [5,6]. In addition, the high pressure and temperature induced by the liquid in the pipeline create internal longitudinal stresses, resulting in pipe-buckling [1]. Oil or gas leakage induced by pipeline damage can cause serious disasters in the ocean's ecological environment. For example, continuous oil leaks may lead to the failure of related safety valve, causing gas ignition, explosion, and structural damage with the further release of oil [1,7]. So far, considerable studies have been made to investigate the scour process beneath the submarine pipeline [8–14].

Chiew [15] carried out a series of laboratory experiments to study the mechanism of the onset of scour underneath pipelines. The results indicated that the piping caused by the pressure difference between the upstream and downstream pipeline edges plays a dominant role in the onset of scour below the pipeline. There are three types of scour erosion around a pipeline, including luff scour, lee scour and tunnel scour. According to Chiew [15], luff scour induced by an eddy formation occurs at the upside of the pipeline

and lee scour is mainly caused by the re-emergence of the main flow over and the turbulent wake downstream of the pipeline, and it occurs at the downstream side of the pipeline. Tunnel scour takes place at the lee-side of the pipeline as a result of piping. Sumer et al. [8] videotaped the scour process around the pipeline by a mini underwater camera, indicating that the piping induced by the seepage flow below the pipeline significantly contributes to initial scour. Moreover, the vortex system at upstream and downstream pipeline edges may promote the piping by digging sediments from the seabed. Lu et al. [16] adopted the renormalized group turbulence model (RNG) and large eddy simulation (LES) to study the mechanism of local scour underneath pipelines, respectively. The results instructed that the piping and vortex system around the pipeline contributes to the onset of scour simultaneously. However, without piping, the vortex alone is incapable of initiating tunnel scour beneath the pipeline [15].

For waves, the critical near-bed velocity for the onset of scour below pipeline is generally lower than the case of steady current, meaning that the sediments around the pipeline are easier to be mobilized than the current-only condition [17,18]. The experiments conducted by Fredsøe et al. [19] implied that the lee-wake is closely related to the scour process around the pipeline, and the equilibrium scour depth S_{eq} is mainly governed by KC number. Based on their test results, a theoretical model regarding the S_{eq} and KC was proposed. As reported by Fredsøe et al. [19], for live bed regimes in waves, the scour depth has a weak correlation with Shields number θ and Reynold's number. It should be noted that the scour depth also depends on numerous other factors, such as flow conditions and soil parameters, so caution should be taken when considering the above conclusion. Liu et al. [20] developed a two-dimensional numerical model to calculate the S_{eq}, indicating the higher wave height and wave period usually result in a larger $S_{eq.}$ Fuhrman et al. [21] performed a series of numerical simulations to investigate the scour and backfilling process around the pipeline, showing that the scope of the scour pit is significantly influenced by the new wave climate. Ahmad et al. [13] simulated the scour evolution around the submarine pipeline in combined waves and current, which reveals that the scour depth increases with current velocity for the same KC.

For scour protection below the pipeline, there are usually two types according to their principles: (1) burying the pipeline in sediments and (2) preventing the onset of scour beneath pipethe line [22–25]. As for the first type, the self-burial of the pipeline was utilized to let it embed in the seabed. The mechanism and detailed process of self-burial for pipelines in waves can refer to Sumer et al. [8]; as the scope of scour hole becomes larger, the span shoulders get shorter, and the soil bears more weight of the pipeline. Once the bearing capacity of the soil is exceeded, the pipeline begins to sink, leading to the self-burial. The equilibrium self-burial depth is a key parameter for scour protection design, and it has a strong correlation with KC. The self-burial process can be facilitated by installing a rigid spoiler on the top surface of the pipeline [9]. The spoiler enlarges the cross-section of the pipeline, and increases the turbulence intensity around it, thus leading to more sediments being mobilized, leading to the scour depth being enhanced. Therefore, the self-burial process can be promoted by installing a spoiler, and consequently, the pipeline can be buried in the seabed. It is noteworthy that the spoiler may cause vortex-induced vibration due to increasing turbulence intensity, and therefore lead to pipeline failure. What is more, the sediments erosion rate varies greatly along the pipeline because of the discrepancy of soil properties, which will cause pipeline suspension in the local regions, so it still needs further improvement in practice. The latter countermeasure is mainly placing protection materials or installing additional structures adjacent to the pipeline, such as gravels, rocks, geotextiles, concrete mattresses, impermeable rigid (or rubble) plates [9,10,26–28]. These measures effectively reduce the pressure gradient beneath the pipeline, and consequently, the piping is hard to occur. In this way, the sediments below the pipeline may not be carried away and transported. Xie and Liu [29] proposed a new flexible protection structure to prevent scour, which is composed of a geotextile mattress and a sloping curtain (GMSC). The GMSC can be applied to protect the riverbed and banks from scour with good performance; after

that, the GMSC was installed in vicinity of the pipeline to mitigate scour. The scour tests were carried out in a regular flume with a scale of 1:35 and the results indicated the GMSC can effectively decrease the hydraulic pressure across the pipeline and thus piping was difficult. Recently, Zhu et al. [30] developed an innovative device, named GMFP, to relieve scour around pipelines. The GMFP includes a supporting foundation and a floating plate. A geotextile mattress can be used as the supporting foundation, which is constituted of a string of tubes filled with solid materials, such as sand, pebbles, concrete blocks, and so on. A series of laboratory tests were conducted to study the protective effects of GMFP for scour below pipeline in unidirectional current, and the results instructed that the GMFP can effectively inhibit the onset of scour by significantly reducing the hydraulic gradient beneath pipeline. However, these scour prevention devices increase the cost to some extent, and it may be difficult to install these devices in exact places. Furthermore, once these devices were installed on the seabed, they will suffer the lasting cyclic loading induced by waves and current, so it is still a challenge to make sure the stability in service life.

Motivated by this, an innovative approach, using the Ionic Soil Stabilizer (ISS) solidified slurry as scour protection layer, was proposed to prevent scour around the pipeline. The ISS-solidified slurry adopted in the present study is constituted of ISS, Dispersion Resistance Agent (DRA), silty clay, and distilled water. The ISS solution includes cations and anions (e.g., Na^+, Mg^{2+}, Ca^{2+}, $NO_3{}^-$ and $(SO_4)^{2-}$). The concentration of main cations and anions is as follows: Na^+: 40.86 mg/L; Mg^{2+}: 40.83 mg/L; Ca^{2+}: 49.1 mg/L; $NO_3{}^-$: 42.32 mg/L; $(SO_4)^{2-}$: 45.22 mg/L. As for inland engineering, the ISS-solidified soil was generally used for ground improvement because it is cost-effective and eco-friendly [31,32]. The ISS-solidified slurry can be poured adjacent to the pipeline immediately after the pipeline was placed, or in the growing scour holes (see Figure 1). In the present study, the first type was utilized as the scour protection layer around the pipeline. The organization of the present study can be summarized as follows. Firstly, a series of laboratory flume tests were carried out to verify the adaption and protective effects of the ISS-solidified slurry for the pipeline. After that, the mechanism of the ISS-solidified slurry for scour protection beneath the pipeline was analyzed by the scanning electron microscope (SEM) tests and pore size tests, respectively. Furthermore, the effects of the ISS-solidified layer for liquefaction stability of non-cohesive subsoil were evaluated. Finally, the performance of ISS-solidified slurry as scour protection layer was discussed comprehensively.

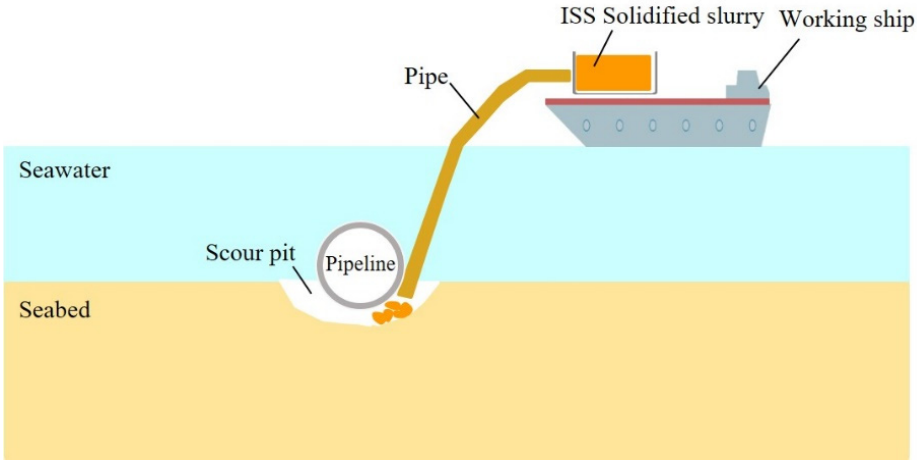

Figure 1. Schematic of construction procedure of ISS-solidified slurry in the field.

2. Tests Design

A series of laboratory tests were designed to validate the protective capacity of ISS-solidified slurry for pipeline in waves and combined waves and current, which were conducted in a wave-current flume with the dimensions 14 m × 1 m × 1.5 m (Figure 2, length × width × height) of Ocean University of China. A wave generating device was

set on one side of the flume, which is composed of an electric controller, wave maker, and a piston rod. The wave absorption band with a length of 2 m and an inclination of 14° was placed on the other side of the flume, and it was made of gravel and rubble. A rectangle soil pit (1.4 m in length, 0.5 m in height) was installed in the center of the flume. The pipeline model is made of Polyvinyl chloride (PVC), and the diameter D is 2.5 cm. In experiments, the pipeline model was resting on the seabed without any gap, and it was rigidly fixed in whole scour tests to avoid the sagging of the pipeline. The wave height gauges were set on the upstream section close to the pipeline model, and the Acoustic Doppler Velocimeter (ADV) was adopted to acquire the near-bed velocity with a distance of 5 cm (2 D) above the seabed. In order to obtain the instantaneous scour depth, the scour probes were installed vertically on the bottom of the pipeline. The evolution of the scour pit in tests was videotaped by a camera, so the whole process for the onset of the scour and scour evolution can be monitored and recorded completely. The Figure 3 depicts the particle size grading curve of the sandy silt, and it was used as the initial (untreated) seabed. The physical parameters of the soil sample can be summarized as follows. The specific gravity of soil particle G_s = 2.64, the median diameter d_{50} = 0.051 mm, the plastic limit ω_P = 17.1%, liquid limit ω_L = 26.3%, porosity n = 0.41, permeability coefficient $k_s = 1.0 \times 10^{-5}$ m/s, shear modulus $G = 5.0 \times 10^5$ Pa, Possion's ratio ν = 0.28.

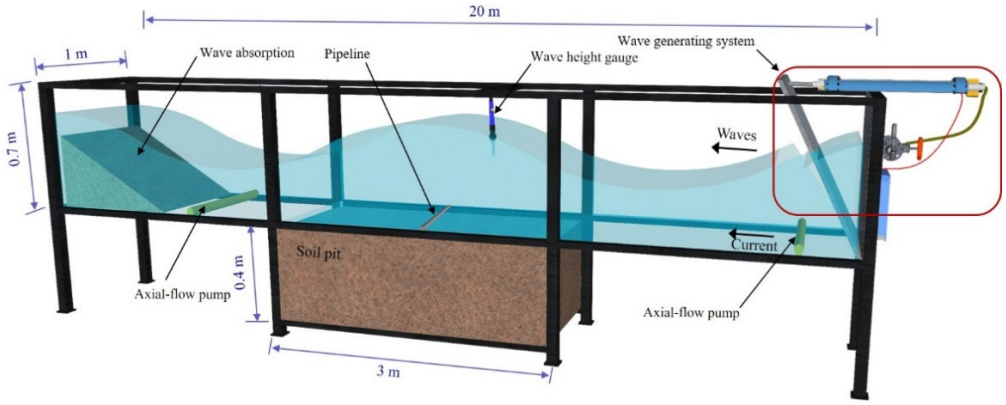

Figure 2. Schematic of experimental setup.

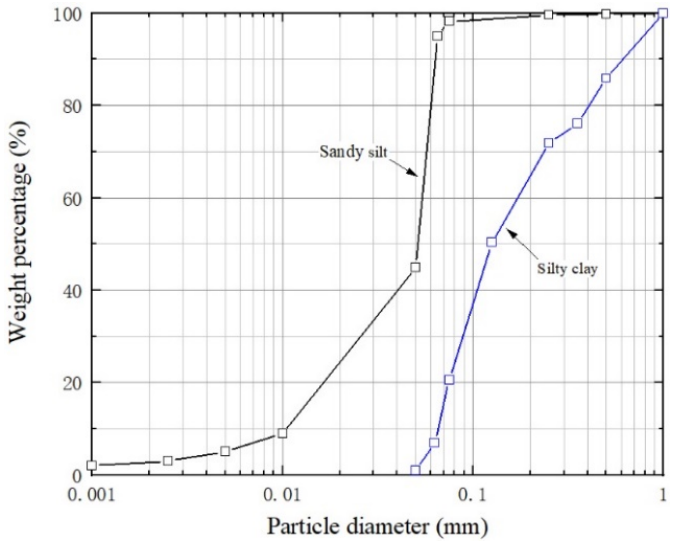

Figure 3. Grain size distribution curves of the sandy silt and silty clay for untreated and ISS-solidified seabed, respectively.

The ISS-solidified slurry adopted in present study includes the ISS, DRA, silty clay and distilled water. Before being solidified by ISS, the silty clay was dried, crushed, and

passed through a 1 mm sieve. Figure 3 illustrates the particle size grading curve of the silty clay. For silty clay used in experiments, the specific gravity G_s = 2.76, the median diameter d_{50} = 0.131 mm, plastic limit ω_P = 21.2%, liquid limit ω_L = 25.8%. The ISS is a light gray liquid, soluble in distilled water to form ISS solution based on the design mixture ratio. The DRA is a gray solid powder, which is made of crystalline polymer and polymeric surfactant, etc. It can be expected that the different design mixture ratios of ISS-solidified slurry will result in the discrepancy of scour protection effects, so three kinds of ISS-solidified slurry (see Table 1) were utilized as scour protection layer around the pipeline. According to the design mixture ratio, we mixed the needed silty clay and DRA together, then add ISS solution. After that, we poured the ISS-solidified slurry at upstream and downstream of the pipeline's edges (see Figure 4) to a length of 7.5 cm (3 D) on each side and a thickness of 1.25 cm (0.5 D).

The scour experiments were performed immediately after the scour protection layer being built. The detailed test parameters are given in Table 1. The water depth d was 40 cm, and it stayed consistent in all tests. The regular waves were employed with wave height H_w ranging from 6 cm to 12 cm. The test duration for all tests is 30 min (1200 wave cycles). Taking H_i and H_r as the height of the incident wave and reflected wave, respectively, the reflection coefficient $K_r = H_r/H_i$ in present tests was found to be less than 10% due to the installation of the wave absorption band, so the wave reflection was negligible. The $(S/D)_{max}$ in Table 1 represents the maximum dimensionless scour depth beneath the pipeline in tests.

Table 1. Summary of experimental parameters for the untreated seabed and ISS-solidified seabed.

Type	Mix Proportion	Run Number	H_w (m)	T (s)	U_c (m/s)	U_{cw}	KC	θ	$(S/D)_{max}$
Untreated (Initial) seabed (INI)	Sandy silt (in Figure 2)	INI-1	0.06	1.5	0	0	5.87	0.04	0.26
		INI-2	0.08	1.5	0	0	7.82	0.07	0.3
		INI-3	0.10	1.5	0	0	9.78	0.09	0.33
		INI-4	0.08	1.5	0.16	0.45	7.82	0.07	0.32
		INI-5	0.10	1.5	0.16	0.41	9.78	0.11	0.35
		INI-6	0.12	1.5	0.16	0.30	11.73	0.12	0.36
ISS-solidified seabed (ISS-A)	V_{ISS}:V_{water} = 1:20 M_{DRA}:$M_{ISS\ solution}$:$M_{silty\ clay}$ = 1:10:20	ISS-A-1	0.06	1.5	0	0	5.87	0.04	0.062
		ISS-A-2	0.08	1.5	0	0	7.82	0.07	0.071
		ISS-A-3	0.10	1.5	0	0	9.78	0.09	0.085
		ISS-A-4	0.08	1.5	0.16	0.45	7.82	0.07	0.079
		ISS-A-5	0.10	1.5	0.16	0.41	9.78	0.11	0.096
		ISS-A-6	0.12	1.5	0.16	0.30	11.73	0.12	0.102
ISS-solidified seabed (ISS-B)	V_{ISS}:V_{water} = 1:20 M_{DRA}:$M_{ISS\ solution}$:$M_{silty\ clay}$ = 1:5:9	ISS-B-1	0.06	1.5	0	0	5.87	0.04	0.012
		ISS-B-2	0.08	1.5	0	0	7.82	0.07	0.019
		ISS-B-3	0.10	1.5	0	0	9.78	0.09	0.031
		ISS-B-4	0.08	1.5	0.16	0.45	7.82	0.07	0.028
		ISS-B-5	0.10	1.5	0.16	0.41	9.78	0.11	0.043
		ISS-B-6	0.12	1.5	0.16	0.30	11.73	0.12	0.045
ISS-solidified seabed (ISS-C)	V_{ISS}:V_{water} = 1:20 M_{DRA}:$M_{ISS\ solution}$:$M_{silty\ clay}$ = 1:3:6	ISS-C-1	0.06	1.5	0	0	5.87	0.04	≈0
		ISS-C-2	0.08	1.5	0	0	7.82	0.07	≈0
		ISS-C-3	0.10	1.5	0	0	9.78	0.09	0.011
		ISS-C-4	0.08	1.5	0.16	0.45	7.82	0.07	0.009
		ISS-C-5	0.10	1.5	0.16	0.41	9.78	0.11	0.013
		ISS-C-6	0.12	1.5	0.16	0.30	11.73	0.12	0.015

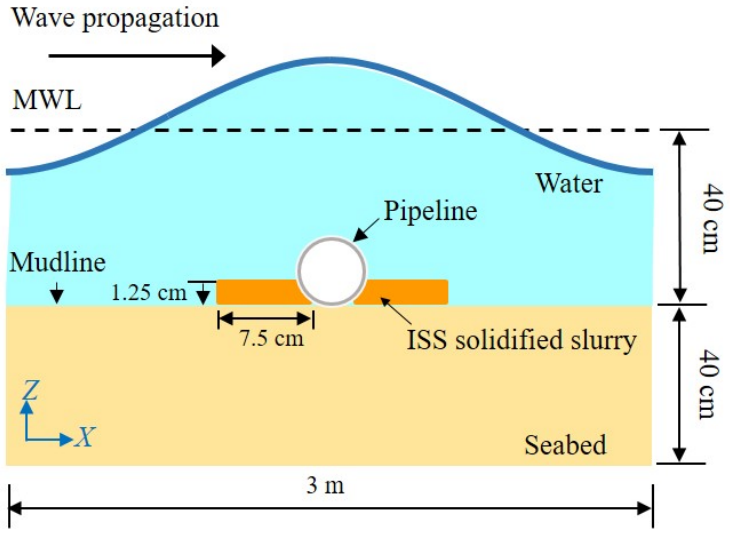

Figure 4. Arrangement of ISS-solidified slurry. (MWL-mean seawater line).

In Table 1, the KC was obtained from the following equation [33]:

$$\mathrm{KC} = \frac{U_{\mathrm{wm}} T}{D} \tag{1}$$

Where, T the wave period, U_{wm} the maximum near-bed velocity of the undisturbed wave-induced oscillatory flow.

The current to wave velocity ratio U_{cw} was computed as [33]:

$$U_{\mathrm{cw}} = \frac{U_{\mathrm{c}}}{U_{\mathrm{wm}} + U_{\mathrm{c}}} \tag{2}$$

Where U_{c} is the undisturbed near-bed velocity of the current component.

The Shields parameter was calculated as [34]:

$$\theta = \frac{U_{\mathrm{f,m}}^2}{(\rho_{\mathrm{s}}/\rho_{\mathrm{w}} - 1) g d_{50}} \tag{3}$$

Where, $U_{\mathrm{f,m}}$ *is* the maximum near-bed friction velocity, g is the gravity acceleration, ρ_{s} the density of the sediment; ρ_{w} is the fluid density.

The critical Shields parameter θ_{cr} for the sediment's initial motion was acquired from the following equation [34]:

$$\theta_{\mathrm{cr}} = \frac{0.3}{1 + 1.2 d_*} + 0.055[1 - \exp(-0.02 d_*)] \tag{4}$$

$$d_* = \left[\frac{(\rho_{\mathrm{s}}/\rho_{\mathrm{w}} - 1)\mathrm{g}}{v^2}\right]^{1/3} \tag{5}$$

Where ν is the kinematic viscosity of the fluid.

The relationship between θ and θ_{cr} satisfies $\theta > \theta_{\mathrm{cr}}$ in all tests, meaning that the live bed scour develops. The model scale of prototype value to model value is 1:40. In laboratory scour tests, it is typically impossible to ensure the Froude similarity of all parameters between the prototype and model, leading to the scale effects in model tests [35]. For example, the sediments were not scaled according to the geometrical size. As a result, it causes the underestimated of suspended load transport and overestimated of bed load transport [36]. In addition, the disproportional scaled sediments also contribute to the difference in bed roughness between prototype and model, thereby the obvious impacts on the near-bed boundary layer and scour temporal development.

3. Scour Process and Scour Profile

The whole scour process was obtained by the video. Figure 5 depicts the schematic of the scour process around the pipeline at different times based on the videotape. When a pipeline was placed on an erosion seabed in waves or current, a seepage flow formed beneath the pipeline due to the pressure difference between the upstream and downstream pipeline edges (see Figure 5a). A critical state was reached when the pressure gradient in the seabed at the downstream pipeline edges equaled the flotation gradient of soil grains. Once the critical state was exceeded, the surface of sediments began to rise at the downstream pipeline's edge (Figure 5b). With the lasting actions of waves and current, a mixture of sediments and fluids would have broken through and jetted from the seabed (Figure 5c), meaning piping occurred, which indicates the onset of scour beneath the pipeline. According to Mao [37], there are three types of vortexes (see Figure 5a) existing in vicinity of the pipeline, called stagnation eddy (Vortex A) at the upside, lee-wake vortex (Vortex B) and anticlockwise small vortex (Vortex C) at the downside. Vortex A significantly increases the turbulence intensity at the upstream pipeline edges while Vortex C can sweep away the sediments from seabed, so it promotes the initial scour to some extent. Therefore, it can be believed that the combination of piping and vortex system contribute to the onset of scour around the pipeline; however, the experiment, with an impermeable plate paced at the upside of pipeline conducted by Chiew [15], revealed that the vortex system alone was incapable of causing the onset of scour, so the initial scour beneath pipeline was mainly governed by piping. Based on that, it was concluded that the scour could be prevented if the piping process underneath the pipeline was effectively controlled.

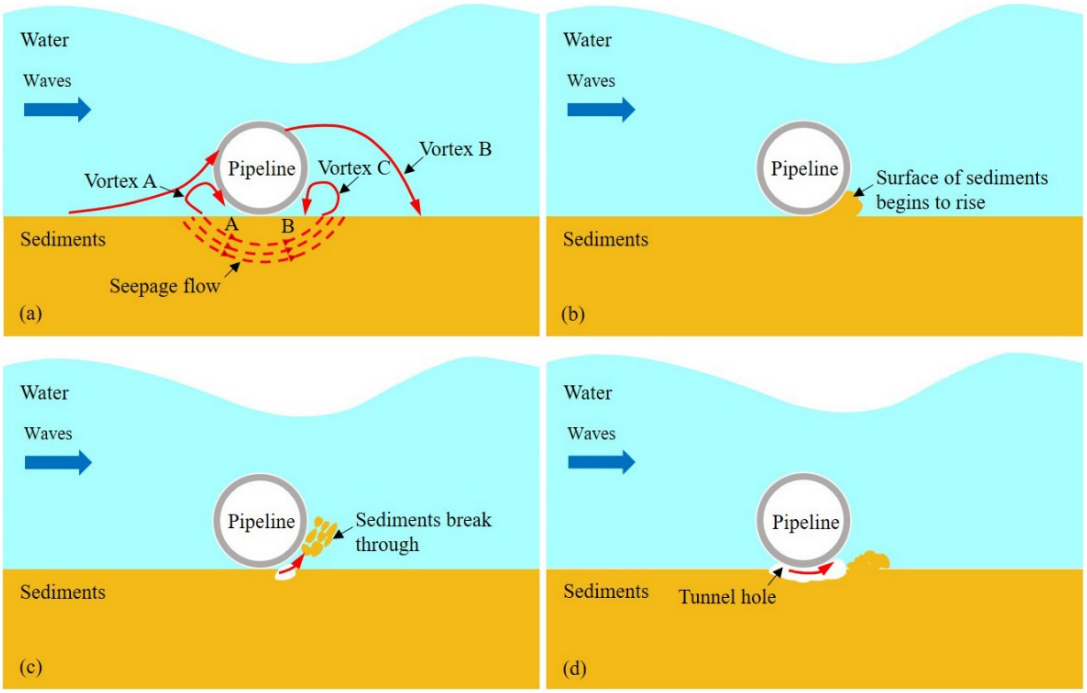

Figure 5. Schematic of scour process in experiments.

It is noteworthy that the breakthrough of sediments in Figure 5c at the lee-side of pipeline was a progressive process, and each wave cycle disturbed and loosen some soil particles on the exiting side [8]. The breakthrough process mainly depended on the soil porosity, internal frication, and length of the seepage flow path [2,8,19]. Compared with the initial seabed, the ISS-solidified seabed needed more time, i.e., suffered more wave cycles, to make a breakthrough. For example, for case INI-1, it required about 10 s (about 7 wave cycles) to reach a breakthrough point, but for case ISS-A-1, the breakthrough occurred when t = 60 s, and for ISS-C-1, there was no breakthrough even if it suffered 1200 wave

cycles, and as a result, no piping occurred. The results indicated that if a proper design mixture ratio is chosen for ISS-solidified slurry, it can work perfectly to prevent the piping beneath the pipeline.

Once the piping was triggered, the scour would further develop rapidly, leading to a tunnel scour hole (see Figure 5d) appearing between the pipeline and seabed. The flow velocity in the tunnel scour hole was significantly larger than the undisturbed flow velocity far away from the pipeline [2], so the sediments still jetted from the tunnel scour hole in this stage. With the gap between pipeline and seabed developing, the enhancement of the flow velocity in the tunnel's scour hole decreased. The maximum scour depth was reached when the flow velocity in the tunnel scour hole became the same as the undisturbed flow velocity. As the gap further developed, the lee-wake vortex shed off at the downstream side of the pipeline. The lee-wake vortex dragged and transported sediments away from the pipeline and deposited the sediments at the lee-side. Figure 6 shows the final scour morphology in tests around the pipeline for case INI-5, ISS-B-1 and ISS-C-1, respectively.

(**a**)

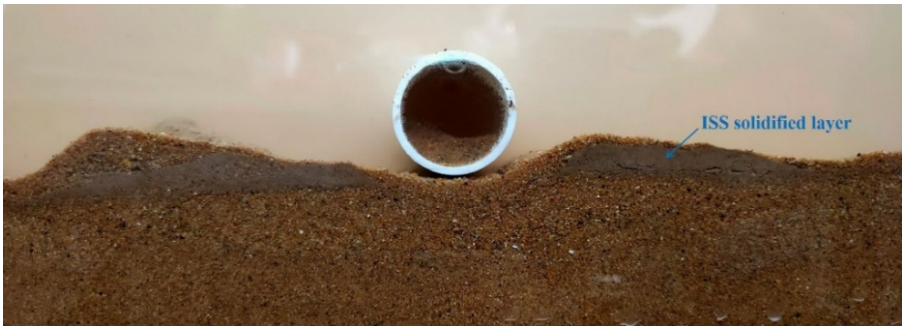

(**b**)

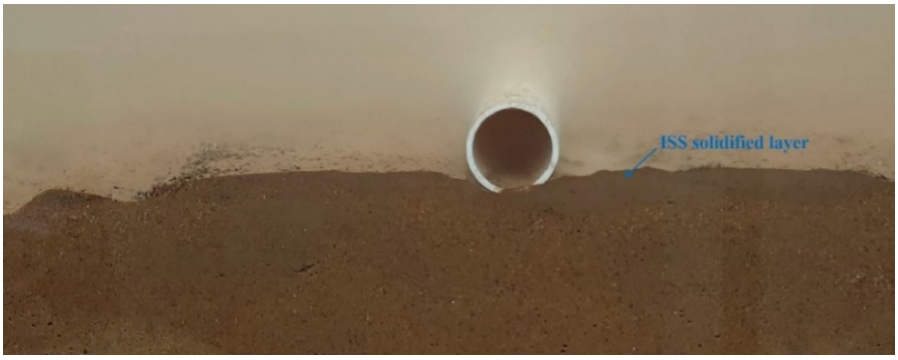

(**c**)

Figure 6. Scour profiles at the end of tests: (**a**) Untreated seabed (case INI-5), (**b**) ISS-solidified seabed (case ISS-B-1), (**c**) ISS-solidified seabed (case ISS-C-1).

For initial seabed INI-5, the scour profile appeared asymmetrical with a greater accretion height, which is similar to that reported by Sumer et al. [8], Larsen et al. [12], and Xu et al. [38]. For the ISS-solidified seabed ISS-B-1, there was only a tiny tunnel scour hole beneath the pipeline, and the maximum scour depth $(S/D)_{max}$ was 0.012 with about 96.6% smaller than the case of INI-1. As discussed in the above section, if a proper design mixture ratio is chosen for ISS-solidified slurry, it can prevent the onset of scour beneath the pipeline by inhibiting piping. It should be noted the lee-wake vortex always existed, although no piping occurred for the ISS-solidified seabed, so it can be expected that the scour hole still appeared at the lee-side of the pipeline. But for ISS-C-1, there was almost no evident scour hole in the vicinity of the pipeline, indicating that the ISS-solidified slurry also can protect the seabed from scour induced by the lee-wake vortex. In general, based on the experimental results, the protective effects of ISS-solidified slurry for pipelines are favorable.

4. Mechanism of ISS for Scour Protection Beneath Pipeline

According to Sumer et al. [8], the critical condition for the onset of scour beneath the pipeline can be expressed by the pressure difference between the upstream and downstream pipeline edges.

$$\frac{\partial}{\partial x}\left(\frac{P}{\gamma}\right) \geq (s-1)(1-n) \tag{6}$$

$$\frac{\partial}{\partial x}\left(\frac{P}{\gamma}\right) = \frac{P_A - P_B}{\overline{AB}} \tag{7}$$

$$s = \frac{\gamma_s}{\gamma} \tag{8}$$

Where, $\frac{\partial P}{\partial x}$ the pressure gradient leading to the seepage flow beneath the pipeline, P_A and P_B the pressure at points A and B in Figure 5a; s is the specific gravity of soil grains, γ_{is} the specific weight of water, γ_s is the specific weight of soil grains, and n the soil porosity.

As discussed in Section 3, for ISS-C-1, there was no initial scour beneath the pipeline, indicating the critical condition described in Equation (6) cannot be satisfied. For the given hydraulic parameters and pipeline sizes, the $\frac{\partial P}{\partial x}$ is the same. What is more, the difference of s is relatively small between the initial seabed and the ISS-solidified seabed. Therefore, it can be reasonably inferred that the ISS-solidified slurry enhances the critical pressure gradient for initial scour underneath the pipeline by decreasing the soil porosity n.

Thus, the scanning electron microscope (SEM) tests were carried out to study the change in the microstructure of soil grains for untreated and ISS-solidified soil samples, respectively. The process of SEM tests can be summarized as follows. (1) Make the cylindrical sample with the dimensions 50 mm × 50 mm (diameter × height) and dry it in the air. (2) Cut the dried soil sample into a cubic shape with the dimensions 10 mm × 10 mm × 5 mm (length × width × height). (3) Tear the soil sample carefully by tweezer to obtain the undisturbed soil structural plane. Then, put the soil sample in a vacuum evaporation coaster with the undisturbed soil structural plane facing up. (4) Spray gold film on the soil sample surface to make sure there is excellent electrical conductivity. The microstructures of the soil samples were observed by a SEM. Figure 7 shows the SEM images for the untreated and ISS-solidified soil sample under 5000 times magnification.

As shown in Figure 7, for the untreated soil, the soil particles emerge as a small aggregation and loose stack of clay platelets. For ISS-solidified soil, the clay platelets aggregate together and form into much larger grain clusters. Figure 8 gives the binary SEM photos for the untreated and ISS-solidified soil samples. The white and black regions in Figure 8 represent soil grains and pores, respectively. Compared with an untreated soil sample, the amount and size of pores decrease significantly, indicating the soil becomes denser after being solidified.

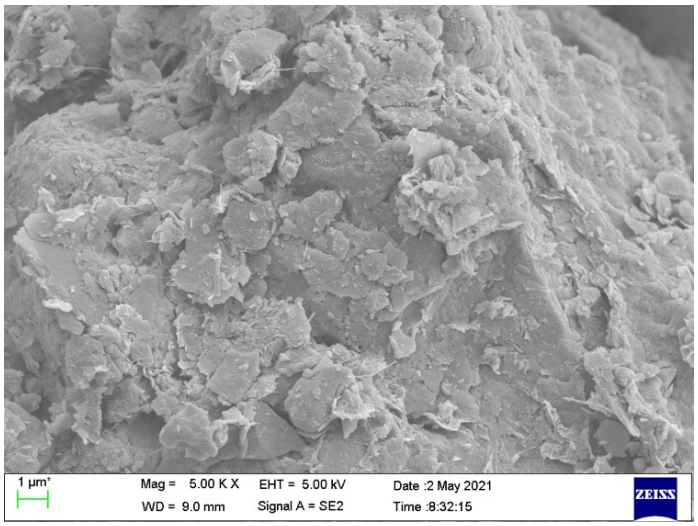

(**a**)

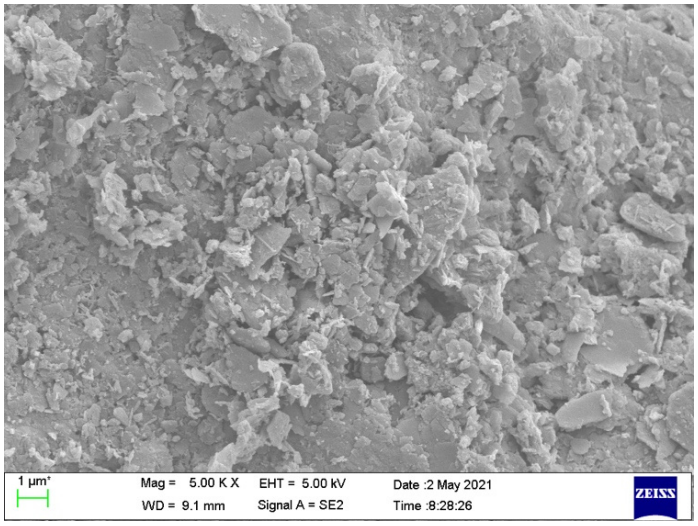

(**b**)

Figure 7. The SEM photos for the untreated and ISS-solidified soil sample: (**a**) untreated soil sample (INI), (**b**) ISS-solidified soil sample (ISS-A).

In order to further evaluate the pore volume for the untreated and ISS-solidified soil sample, the pore size tests were conducted. The samples used in pore size tests are same as the SEM tests. The steps for pore size tests are listed below. (1) Crust the dry soil sample and pass through a 0.25 mm sieve. (2) Shift the soil sample into a vacuum machine and vacuumize the specimen. (3) Put the soil sample into the pore size analyzer to test the pore volume. Figure 9 shows the pore volume for the untreated and ISS-solidified soil samples under different pressures.

The P_i and P_{ini} in Figure 9 denote the experimental and atmospheric pressure, respectively, and V_v denotes the pore volume in the soil sample. From Figure 9, compared with the untreated soil, the V_v decreased evidently for the ISS-solidified soil, instructing that the soil porosity $n = V_v/V$, (V the volume of soil sample) diminished. According to Equation (6), the smaller n will result in the enhancement of critical condition for the onset of scour beneath pipeline, and the ISS-solidified soil will get more resistance to piping, so the seabed around pipeline can be protected against scour.

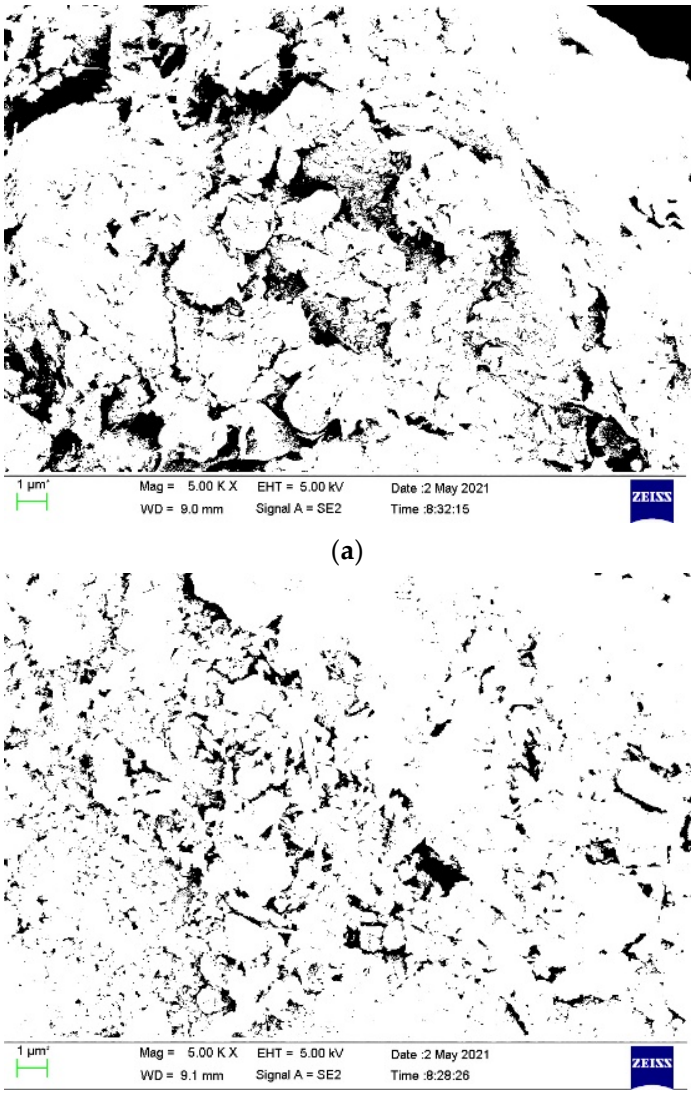

Figure 8. The binary SEM photos for the untreated and ISS-solidified soil sample: (**a**) Untreated soil sample, (**b**) ISS-solidified soil sample (ISS-A).

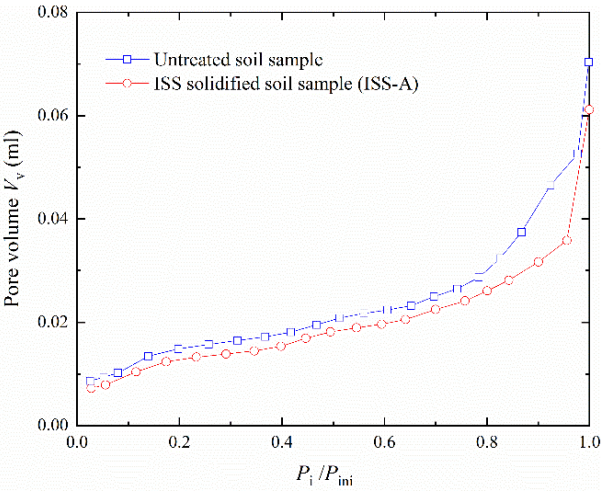

Figure 9. The results of pore size tests.

Furthermore, as described in Section 3, when the shear stress τ_c induced by lee-wake exceeds the critical shear stress τ_{cr} for sediments initial motion, the lee-wake will drag and transport sediments, so the lee-wake vortex can also lead to scour at the downstream pipeline edge. According to Smerdon and Beasley [39], the relationship between the critical shear stress τ_{cr} for the initial scour and the plasticity index I_p can be expressed as:

$$\tau_{cr} = 0.0034 I_P^{0.84} \quad (9)$$

In present tests, the I_{p1} = 4.6 for the untreated soil sample, and the I_{p1} = 9.2 for the ISS-solidified soil sample (ISS-C). Based on Equation (9), the greater I_p will lead to the larger τ_{cr}. Consequently, the critical shear stress required for initial scour increased for the ISS-solidified soil, so the ISS-solidified soil needed to overcome the greater shear stress for incipient scour. In general, the ISS can both prevent the onset of scour (i.e., piping) underneath the pipeline by decreasing soil porosity and inhibiting the scour induced by the vortex system around the pipeline by enhancing the critical shear stress.

5. The Effects of ISS-solidified Layer for Liquefaction around the Pipeline

5.1. Experiments Design

The ISS-solidified layer has a dense structure and greater shear modulus, so it likes a crust layer, and if a non-cohesive soil layer exists underneath the ISS-solidified layer, it may inhibit the dissipation of pore pressure and result in the buildup of pore pressures that can cause accumulated liquefaction. Therefore, it is vital to further evaluate the effects of the ISS-solidified layer for liquefaction stability of non-cohesive subsoil. The experiments were conducted in a wave flume. The flume, soil, pipeline model, and production process of the ISS-solidified soil are the same as Section 2, and it will not be repeated here. To obtain the instantaneous pore pressure in the seabed, the pore pressure gauges were placed in seabed before tests, and the layout of pore pressure gauges was shown in Figure 10. Table 2 lists the test plan and detailed test parameters. The water depth d was 40 cm, and it stayed consistent in all tests. The regular waves were employed with wave height H_w ranging from 6 cm to 18 cm. According to the liquefaction criterion deduced by Zen and Yamazaki [40], when the accumulated pore pressure P_{res} exceeded the mean normal effective stress σ_0', i.e., $P_{res}/\sigma_0' \geq 1$, the liquefaction occurred. The cycle stress ratio χ for every case was computed by the following equation based on Sassa and Sekiguchi [41].

$$\chi = \frac{kP_0}{\gamma'} \quad (10)$$

where k the wave number, P_0 the pore pressure amplitude induced by waves on seabed surface, γ' the submerged weight of soils.

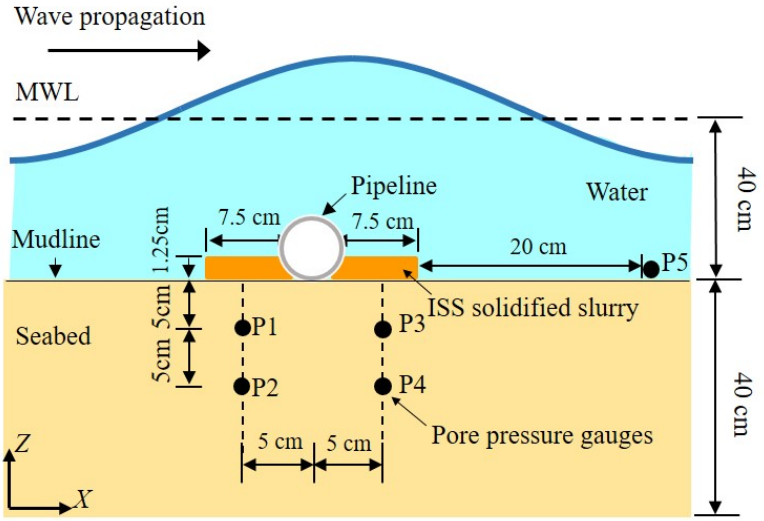

Figure 10. Arrangement of pressure gauges and ISS-solidified slurry.

Table 2. Summary of experimental parameters for the untreated seabed and ISS-solidified seabed.

Type	Mix Proportion	G (Pa)	Ks (cm/s)	Run Number	H_w (m)	χ
Untreated seabed (INI)	Sandy silt (in Figure 2)	5.0×10^5	1.0×10^{-5}	INI-7	0.06	0.099
				INI-8	0.08	0.132
				INI-9	0.10	0.165
				INI-10	0.12	0.198
				INI-11	0.14	0.231
				INI-12	0.16	0.264
				INI-13	0.18	0.297
ISS-solidified seabed (ISS-A)	V_{ISS}:V_{water} = 1:20 M_{DRA}:$M_{ISS\ solution}$:M_{clay} = 1:10:20	5.8×10^5	1.0×10^{-6}	ISS-A-7	0.06	0.099
				ISS-A-8	0.08	0.132
				ISS-A-9	0.10	0.165
				ISS-A-10	0.12	0.198
				ISS-A-11	0.14	0.231
				ISS-A-12	0.16	0.264
				ISS-A-13	0.18	0.297
ISS-solidified seabed (ISS-B)	V_{ISS}:V_{water} = 1:20 M_{DRA}:$M_{ISS\ solution}$:$M_{silty\ clay}$ = 1:5:9	6.1×10^5	6.8×10^{-7}	ISS-B-7	0.06	0.099
				ISS-B-8	0.08	0.132
				ISS-B-9	0.10	0.165
				ISS-B-10	0.12	0.198
				ISS-B-11	0.14	0.231
				ISS-B-12	0.16	0.264
				ISS-B-13	0.18	0.297
ISS-solidified seabed (ISS-C)	V_{ISS}:V_{water} = 1:25 M_{DRA}:$M_{ISS\ solution}$:$M_{silty\ clay}$ = 1:3:6	6.4×10^5	4.9×10^{-7}	ISS-C-7	0.06	0.099
				ISS-C-8	0.08	0.132
				ISS-C-9	0.10	0.165
				ISS-C-10	0.12	0.198
				ISS-C-11	0.14	0.231
				ISS-C-12	0.16	0.264
				ISS-C-13	0.18	0.297

5.2. Validation of Pore Pressure

In order to validate the instantaneous pore pressure response, the comparison of pore pressure between the test values obtained by P5 (see Figure 10) for case ISS-A-11 and theoretical results calculated according to Jeng [42] was shown in Figure 11. The comparison instructs that the experimental results appear a good agreement with the theoretical values, though there are slight discrepancies at positions of wave crest and trough. In general, the pore pressure gauges used in present tests are capable of capturing the instantaneous pore pressure precisely.

5.3. Liquefaction Evaluation of the Seabed beneath an ISS-solidified Layer

Figure 12 depicts the curves between P_{res}/σ_0' and χ at depth of 0.05 m and 0.1 m. There are two pore pressure gauges in the same depth, and one of the greater P_{res}/σ_0' was adopted in Figure 12. As shown in Figure 12, the initial liquefaction did not occur for the untreated seabed, but it occurred in the non-cohesive seabed underneath the ISS-solidified layer when the cyclic stress ratio χ equaled the critical cyclic stress ratio χ_{cr}. This phenomenon shows that the ISS-solidified slurry likes a dense crust layer, so the pore pressure in the non-cohesive seabed has difficulty dissipating, consequently resulting in accumulated liquefaction. For the χ_{cr}, there are obvious discrepancies between the different types of ISS-solidified slurry, indicating the χ_{cr} is closely related to the mixture ratio of

ISS-solidified slurry. For example, the χ_{cr} for case ISS-A is significantly larger than that of case ISS-B. Moreover, the χ_{cr} varies with depth, and the deeper depth generally required the relative greater χ_{cr}. In practice, the effects of accumulated liquefaction on the non-cohesive seabed beneath the ISS-solidified layer should be considered and designed carefully. For example, to make sure the incipient liquefaction does not occur at a fixed depth, the $\chi < \chi_{cr}$ should be satisfied; otherwise, the mixture ratio of ISS-solidified slurry should be changed until $\chi < \chi_{cr}$ is reached.

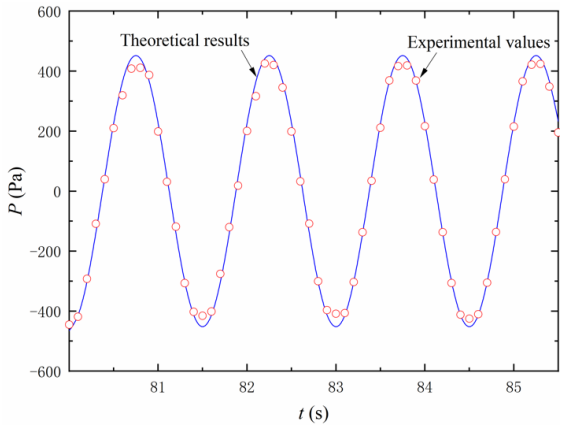

Figure 11. Comparison between experimental values measured by P5 and theoretical results for pore pressure induced by waves.

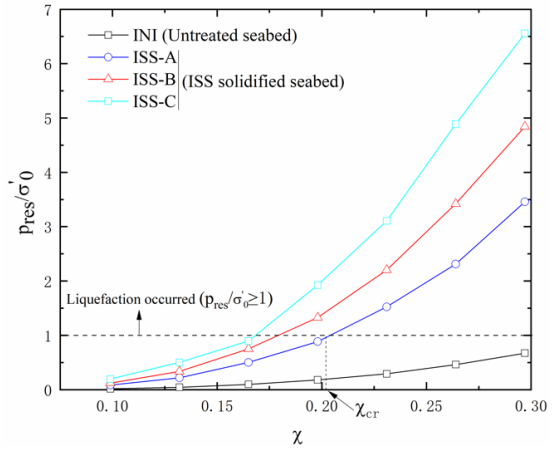

(**a**) 0.05 m

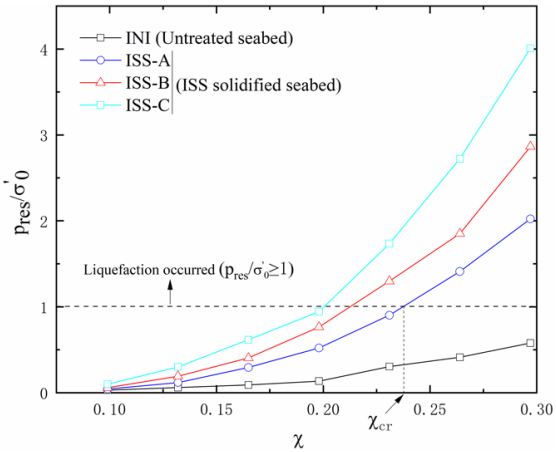

(**b**) 0.1 m

Figure 12. Liquefaction evaluation at different depths.

6. Remark of ISS-solidified Layer for Scour Protection around the Pipeline

As for inland engineering, the ISS-solidified soil was generally used for ground improvement because of its cost-effective and eco-friendly [31,32]. But for ocean environment, when the ISS-solidified slurry was poured in scour pits, it may damage the habitats of benthic fauna that need soft soil to hide from predators, so it is necessary to further conduct an eco-friendly evaluation for benthic fauna. Compared with the countermeasure of placing protection materials or installing additional structures adjacent to the pipeline [25,27], the ISS-solidified slurry is a novel attempt for scour protection around the pipeline. As for other types of marine structures, e.g., monopiles and marine energy structures, the ISS-solidified slurry can also be used as a scour protection layer around the fixed foundations, and can be poured adjacent to the foundations immediately after the foundations were installed, or in the growing scour holes. In August 2019, a Chinese power investment corporation adopted the ISS-solidified slurry as scour protection layer around the monopile of offshore wind turbines (OWTs) in North Binhai District, East China Sea. The results proved the scour around the monopile was effectively prevented, instructing that the ISS-solidified slurry is a quite valid, economic strategy for scour protection around foundations. In the present study, the ISS-solidified slurry was used as the scour protection layer around the pipeline in waves and combined waves and current.

Firstly, a series of laboratory tests were designed to validate the protective capacity of ISS-solidified slurry for the pipeline in waves and combined waves and current. The results revealed that the protective effects of ISS-solidified slurry for pipelines are favorable. According to Cheng [6], Chiew [15], Sumer and Fredsøe [33], and Gao [43], there are some discrepancies in the mechanisms of scour between the single pile and pipeline, especially for the onset of scour. Given this, the SEM tests and pore size tests were conducted respectively to investigate the mechanism of ISS-solidified slurry for scour protection layer around the pipeline. Based on testing results, the ISS can both prevent the onset of scour (i.e., piping) underneath the pipeline by decreasing soil porosity and inhibiting the scour induced by the vortex system around the pipeline by enhancing the critical shear stress for initial scour. Therefore, the ISS-solidified slurry provides an effective treatment for scour protection around the pipeline.

In present scour experiments, the performance of ISS-solidified slurry was tested and evaluated only in regular waves. Noteworthy is that the real waves in the field are quite complicated, so further rigorous validations and calibrations should be conducted in irregular waves or extreme wave conditions before the ISS-solidified slurry was adopted in the field. In addition, the tests were only carried out in relatively lower ranges of U_{cw} due to the limit of the experimental setup, so extra experiments are valuable for larger ranges of U_{cw} in the following studies [44,45]. The ISS-solidified layer has a dense structure and it likes a dense crust layer around the pipeline. If a non-cohesive soil layer exists underneath the ISS-solidified layer, the ISS-solidified layer will inhibit the dissipation of pore pressure, causing the buildup of pore pressures, consequently resulting in accumulated liquefaction. The adverse effects of accumulated liquefaction should be considered carefully due to the set of ISS-solidified layers. On the premise that the scour protective effects of ISS-solidified layer are ensured, it is suggested that to adjust the mixture ratio of the ISS-solidified slurry until the $\chi < \chi_{cr}$ is satisfied at a fixed depth. In general, the ISS-solidified slurry is a reliable, economic approach for scour protection around pipelines in the ocean environment, and it also brings enlightenment for scour protection in ocean engineering.

7. Conclusions

Based on the above analysis, the main conclusions can be summarized as follows:

(1) Compared with the untreated seabed, there are almost no evident tunnel scour holes beneath the pipeline for ISS-solidified seabed, indicating the protective effects of ISS-solidified slurry for pipelines are favorable.

(2) The SEM tests and pore size tests demonstrate that the soil becomes denser after being solidified. The ISS can both prevent the onset of scour (i.e., piping) underneath the

pipeline by decreasing soil porosity and inhibiting the scour induced by the vortex system around the pipeline by enhancing the critical shear stress.

(3) If a non-cohesive soil layer underlies the ISS-solidified slurry, it is vulnerable to suffer accumulated liquefaction due to the dense crust structure of the ISS-solidified layer, so the adverse effects for accumulated liquefaction should be considered carefully due to the setting of the ISS-solidified layer.

(4) On the premise that the scour protective effects of the ISS-solidified layer are ensured, it is suggested to adjust the mixture ratio of ISS-solidified slurry until the $\chi < \chi_{cr}$ is satisfied at a fixed depth to avoid the accumulated liquefaction.

Author Contributions: Conceptualization, X.W.; data curation, R.H. and H.L. (Hao Leng); formal analysis, X.W. and H.L. (Hongjun Liu); funding acquisition, X.W.; writing—original draft, R.H. and H.L. (Hao Leng); writing—review and editing, X.W. and H.L. (Hongjun Liu). The final manuscript has been approved by all the authors. All authors have read and agreed to the published version of the manuscript.

Funding: This research was funded by the Fundamental Research Funds for the Central Universities (grant number 202061027) and the National Natural Science Foundation of China (grant number 41572247).

Institutional Review Board Statement: Not applicable.

Informed Consent Statement: Not applicable.

Data Availability Statement: The data presented in this study are available on request from the corresponding author.

Conflicts of Interest: The authors declare no conflict of interest.

References

1. Seth, D.; Manna, B.; Shahu, J.T.; Fazeres-Ferradosa, T.; Pinto, F.T.; Rosa-Santos, P.J. Buckling Mechanism of Offshore Pipelines: A State of the Art. *J. Mar. Sci. Eng.* **2021**, *9*, 1074. [CrossRef]
2. Seth, D.; Manna, B.; Shahu, J.T.; Fazeres-Ferradosa, T.; Taveira-Pinto, F.; Rosa-Santos, P.; Pinto, F.V.T. Offshore pipeline buried in Indian coastal clay: Buckling behaviour analysis. *Ships. Offshore Struc.* **2021**, 1–16. [CrossRef]
3. Fredsøe, J. Pipeline–seabed interaction. *J. Waterw. Port Coast. Ocean Eng.* **2016**, *142*, 03116002. [CrossRef]
4. Zhang, Q.; Draper, S.; Cheng, L.; An, H. Time scale of local scour around pipelines in current, waves, and combined waves and current. *J. Hydraul. Eng.* **2017**, *143*, 04016093. [CrossRef]
5. Ahmad, N.; Bihs, H.; Myrhaug, D.; Kamath, A.; Arntsen, Ø.A. Three-dimensional numerical modelling of wave-induced scour around piles in a side-by-side arrangement. *Coast. Eng.* **2018**, *138*, 132–151. [CrossRef]
6. Cheng, L.; Yeow, K.; Zhang, Z.; Teng, B. Three-dimensional scour below offshore pipelines in steady currents. *Coast. Eng.* **2009**, *56*, 577–590. [CrossRef]
7. Fazeres-Ferradosa, T.; Rosa-Santos, P.; Taveira-Pinto, F.; Vanem, E.; Carvalho, H.; Correia, J.A.F.D.O. Advanced research on offshore structures and foundation design: Part 1. *Proc. Inst. Civ. Eng.-Marit. Eng.* **2019**, *4*, 118–123. [CrossRef]
8. Sumer, B.M.; Truelsen, C.; Sichmann, T.; Fredsøe, J. Onset of scour below pipelines and self-burial. *Coast. Eng.* **2001**, *42*, 313–335. [CrossRef]
9. Yang, L.P.; Shi, B.; Guo, Y.K.; Wen, X.Y. Calculation and experiment on scour depth for submarine pipeline with a spoiler. *Ocean Eng.* **2012**, *55*, 191–198. [CrossRef]
10. Yang, L.P.; Shi, B.; Guo, Y.K.; Zhang, L.X.; Zhang, J.S.; Han, Y. Scour protection of submarine pipelines using rubber plates underneath the pipes. *Ocean Eng.* **2014**, *84*, 176–182. [CrossRef]
11. Liang, D.; Cheng, L. Numerical model for wave-induced scour below a submarine pipeline. *J. Waterw. Port. Coast. Ocean. Eng.* **2005**, *131*, 193–202. [CrossRef]
12. Larsen, B.E.; Fuhrman, D.R.; Sumer, B.M. Simulation of wave-plus-current scour beneath submarine pipelines. *J. Waterw. Port. Coast. Ocean Eng.* **2016**, *142*, 04016003. [CrossRef]
13. Ahmad, N.; Bihs, H.; Myrhaug, D.; Kamath, A.; Arntsen, Ø.A. Numerical modelling of pipeline scour under the combined action of waves and current with free-surface capturing. *Coast. Eng.* **2019**, *148*, 19–35. [CrossRef]
14. Zang, Z.; Tang, G.; Chen, Y.; Cheng, L.; Zhang, J. Predictions of the equilibrium depth and time scale of local scour below a partially buried pipeline under oblique currents and waves. *Coast. Eng.* **2019**, *150*, 94–107. [CrossRef]
15. Chiew, Y.M. Mechanics of local scour around submarine pipelines. *J. Hydraul Eng.* **1990**, *116*, 515–529. [CrossRef]

16. Lu, L.; Li, Y.; Chen, B. Mechanism of local scour around submarine pipelines based on numerical simulation of turbulence model. In Proceedings of the 24th International Conference on Offshore Mechanics and Arctic Engineering, Halkidiki, Greece, 12–17 June 2005.
17. Zang, Z.; Cheng, L.; Zhao, M.; Liang, D.; Teng, B. A numerical model for onset of scour below offshore pipelines. *Coast. Eng.* **2009**, *56*, 458–466. [CrossRef]
18. Zang, Z.; Cheng, L.; Zhao, M. Onset of scour below pipeline under combined waves and current. In Proceedings of the 29th International Conference on Offshore Mechanics and Arctic Engineering, Shanghai, China, 6–11 June 2010.
19. Fredsoe, J.; Sumer, B.M.; Arnskov, M.M. Time scale for wave/current scour below pipelines. In Proceedings of the 1st International Offshore and Polar Engineering Conference, Edinburgh, UK, 11–16 August 1991.
20. Liu, M.M.; Lu, L.; Teng, B.; Zhao, M.; Tang, G.Q. Numerical modeling of local scour and forces for submarine pipeline under surface waves. *Coast. Eng.* **2016**, *116*, 275–288. [CrossRef]
21. Fuhrman, D.R.; Baykal, C.; Sumer, B.M.; Jacobsen, N.G.; Fredsøe, J. Numerical simulation of wave-induced scour and backfilling processes beneath submarine pipelines. *Coast. Eng.* **2014**, *94*, 10–22. [CrossRef]
22. Xie, L.; Zhu, Y.; Su, T.C. Scour protection of partially embedded pipelines using sloping curtains. *J. Hydraul. Eng.* **2019**, *145*, 04019001. [CrossRef]
23. Ji, U.; Yeo, W.; Kang, J. Subsidence of riprap protection without filters for different installation types of riprap around a pier in sands. *J. Hydro Environ. Res.* **2013**, *7*, 41–49. [CrossRef]
24. Fazeres-Ferradosa, T.; Welzel, M.; Schendel, A.; Baelus, L.; Santos, P.R.; Pinto, F.T. Extended characterization of damage in rubble mound scour protections. *Coast. Eng.* **2020**, *158*, 103671. [CrossRef]
25. Fazeres-Ferradosa, T.; Taveira-Pinto, F.; Reis, M.T.; das Neves, L. Physical modelling of dynamic scour protections: Analysis of the Damage Number. *Proc. Inst. Civ. Eng.-Marit. Eng.* **2018**, *171*, 11–24. [CrossRef]
26. Xie, L.; Huang, W.; Yu, Y. Experimental study of sediment trapping by geotextile mattress installed with sloping curtain. *Geosynth. Int.* **2013**, *20*, 389–395. [CrossRef]
27. Fazeres-Ferradosa, T.; Chambel, J.; Taveira-Pinto, F.; Rosa-Santos, P.; Taveira-Pinto, F.V.C.; Giannini, G.; Haerens, P. Scour protections for offshore foundations of marine energy harvesting technologies: A review. *J. Mar. Sci. Eng.* **2021**, *9*, 297. [CrossRef]
28. Fazeres-Ferradosa, T.; Taveira-Pinto, F.; Romão, X.; Reis, M.; Neves, L.D. Reliability assessment of offshore dynamic scour protections using copulas. *Wind Eng.* **2019**, *43*, 506–538. [CrossRef]
29. Xie, L.; Liu, S. Stability of sand beds around mattress curtain sets. In Proceedings of the 29th International Conference on Offshore Mechanics and Arctic Engineering, Shanghai, China, 6–11 June 2010.
30. Zhu, Y.; Xie, L.; Su, T.C. Scour Protection Effects of a Geotextile Mattress with Floating Plate on a Pipeline. *Sustainability* **2020**, *12*, 3482. [CrossRef]
31. Xiang, W.; Cui, D.; Liu, Q.; Lu, X.; Cao, L. Theory and practice of ionic soil stabilizer reinforcing special clay. *J. Earth Sci.-China* **2010**, *21*, 882–887. [CrossRef]
32. Lu, X.; Xiang, W. *Experimental Study and Its Mechanism of Ionic Soil Stabilizer for Reinforcing Red Clay in Wuhan*; Wuhan University of Technology Press: Wuhan, China, 2019.
33. Sumer, B.M.; Fredsøe, J. Scour around Pile in Combined Waves and Current. *J. Hydraul. Eng.* **2001**, *127*, 403–411. [CrossRef]
34. Soulsby, R. *Dynamics of Marine Sands*; Thomas Telford Ltd.: London, UK, 1998.
35. Frostick, L.E.; McLelland, S.J.; Mercer, T.G. *Users Guide to Physical Modelling and Experimentation: Experience of the HYDRALAB Network*; CRC Press: Los Angeles, CA, USA, 2019.
36. Sutherland, J.; Whitehouse, R.J.S. *Scale Effects in the Physical Modelling of Seabed Scour*; Technical Report; HR Wallingford: Wallingford, UK, 1998.
37. Mao, Y. Seabed scour under pipelines. In Proceedings of the 7th International Symposium Offshore Mechanics and Arctic Engineering, Houston, TX, USA, 7–12 February 1988.
38. Xu, J.; Li, G.; Dong, P.; Shi, J. Bedform evolution around a submarine pipeline and its effects on wave-induced forces under regular waves. *Ocean Eng.* **2010**, *37*, 304–313. [CrossRef]
39. Smerdon, E.; Beasley, R.P. *The Tractive Force Theory Applied to Stability of Open Channels in Cohesive Soils*; Research Bulletin 715; University of Missouri, Agricultural Experiment Station: Columbia, MO, USA, 1959.
40. Zen, K.; Yamazaki, H. Mechanism of wave-induced liquefaction and densification in seabed. *Soils Found.* **1990**, *30*, 90–104. [CrossRef]
41. Sassa, S.; Sekiguchi, H. Wave-induced liquefaction of beds of sand in a centrifuge. *Geotechnique* **1999**, *49*, 621–638. [CrossRef]
42. Jeng, D.-S. *Porous Models for Wave-Seabed Interactions*; Shanghai Jiao Tong University Press: Shanghai, China, 2013.
43. Gao, F.P. Flow-pipe-soil coupling mechanisms and predictions for submarine pipeline instability. *J. Hydrodyn. Ser. B* **2017**, *29*, 763–773. [CrossRef]
44. Wu, M.; De Vos, L.; Arboleda Chavez, C.E.; Stratigaki, V.; Fazeres-Ferradosa, T.; Rosa-Santos, P.; Taveira-Pinto, F.; Troch, P. Large Scale Experimental Study of the Scour Protection Damage Around a Monopile Foundation Under Combined Wave and Current Conditions. *J. Mar. Sci. Eng.* **2020**, *8*, 417. [CrossRef]
45. Arboleda Chavez, C.E.; Stratigaki, V.; Wu, M.; Troch, P.; Schendel, A.; Welzel, M.; Villanueva, R.; Schlurmann, T.; De Vos, L.; Kisacik, D.; et al. Large-Scale Experiments to Improve Monopile Scour Protection Design Adapted to Climate Change—The PROTEUS Project. *Energies* **2019**, *12*, 1709. [CrossRef]